symmetry

IMPACT FACTOR 2.2

CITESCORE 5.3

Article

Intermittency Analysis in Heavy-Ion Collisions: A Model Study at RHIC Energies

Jin Wu, Zhiming Li and Shaowei Lan

MDPI

https://doi.org/10.3390/sym18010138

symmetry

MDPI

Article

Intermittency Analysis in Heavy-Ion Collisions: A Model Study at RHIC Energies

Jin Wu [1], Zhiming Li [2,*] and Shaowei Lan [3]

[1] College of Physics and Electronic Information Engineering, Guilin University of Technology, Guilin 541004, China; wujin35@glut.edu.cn
[2] Key Laboratory of Quark and Lepton Physics (MOE) and Institute of Particle Physics, Central China Normal University, Wuhan 430079, China
[3] School of Electrical and Mechanical Engineering, Pingdingshan University, Pingdingshan 467000, China; shaoweilan@pdsu.edu.cn
* Correspondence: lizm@mail.ccnu.edu.cn

Abstract

Large density fluctuations near the QCD critical point can be probed via intermittency analysis, which involves measuring scaled factorial moments (SFMs) of multiplicity distributions in relativistic heavy-ion collisions. Intermittency reflects the emergence of scale invariance and self-similar structures, which are closely related to symmetry principles and their breaking near a second-order phase transition. We present a systematic model study of intermittency for charged hadrons in Au+Au collisions at $\sqrt{s_{\mathrm{NN}}}$ = 7.7, 11.5, 19.6, 27, 39, 62.4, and 200 GeV. Using the cascade UrQMD model, we demonstrate that non-critical background effects can produce sizable SFMs and a large scaling exponent if they are not properly removed using the mixed-event subtraction method. To estimate the possible critical intermittency signal in experimental data, we employ a hybrid UrQMD+CMC model, in which fractal critical fluctuations are embedded into the UrQMD background. A direct comparison of the second-order SFM between the model and STAR experimental data suggests that a critical intermittency signal on the order of approximately 1.8% could be present in the most central Au+Au collisions at RHIC energies. This study provides practical guidance for evaluating background contributions in intermittency measurements and offers a quantitative estimate for the critical signal fraction present in the STAR data.

Keywords: QCD critical point; symmetry breaking; intermittency; critical signal fraction; background contribution

Academic Editor: Stefano Profumo

Received: 19 December 2025
Revised: 6 January 2026
Accepted: 7 January 2026
Published: 9 January 2026

1. Introduction

One of the frontier research areas in high-energy nuclear physics is to explore the Quantum Chromodynamics (QCD) phase diagram and locate the critical point [1–6]. The phase structure of matter is fundamentally governed by underlying symmetries and their breaking patterns, which can be systematically represented in a phase diagram. For example, water, governed by electromagnetic interactions, has its phase structure depicted by a two-dimensional diagram of pressure (P) versus temperature (T). Similarly, the phase diagram of strongly interacting matter (QCD phase diagram) is typically represented by a two-dimensional plot of the temperature versus baryon chemical potential (μ_B) [1,5,7].

The first-principles lattice QCD calculations show that at low baryon chemical potential and high temperature, the transition from the quark–gluon plasma (QGP) phase to the hadronic matter phase is a smooth crossover [8]. In this regime, the relevant QCD

symmetries, such as chiral symmetry, are approximately restored without a true phase transition. Meanwhile, model predictions based on QCD theory indicate that at higher baryon chemical potential and low temperature, the transition from the QGP phase to the hadronic phase is a first-order phase transition [9], with an end point on the first-order phase transition boundary known as the QCD critical point [9–11]. Determining the structure of the phase diagram of strongly interacting matter is a significant challenge in heavy-ion physics. Experimentally, this requires observables that are sensitive to the symmetry-breaking patterns and critical fluctuations expected near the critical point. To this end, several major experimental facilities are actively searching for signatures of the QCD critical point, including the RHIC-STAR experiment at BNL [1,12], the SPS-NA61/SHINE experiment at CERN [13,14], the HIRFL-CSR external-target experiment [15], the Compressed Baryonic Matter (CBM) experiment [16] and Nuclotron-based Ion Collider fAcility (NICA) experiment [17].

Upon approaching a critical point, as a remnant of the restoration of chiral symmetry, the critical dynamics of the heavy-ion collision system are expected to develop significant density fluctuations [18–21]. These fluctuations manifest as distinct intermittent behavior, characterized by strong variations in number in the density distribution over small phase space cells. Experimentally, such intermittency can be quantified using scaled factorial moments (SFMs) of particle distributions in transverse momentum space [18,22–24]. Recently, the STAR experiment has reported measurements of intermittency for identified charged hadrons in Au+Au collisions at the center-of-mass energies $\sqrt{s_{\mathrm{NN}}}$ = 7.7–200 GeV, based on data from Phase I of the Beam Energy Scan program at RHIC [24,25]. A clear power-law scaling of the higher-order SFMs with respect to the second-order SFM was observed at all energies after background subtraction. Moreover, in the most central (0–5%) collisions, a scaling index ν exhibits a non-monotonic energy dependence, reaching a minimum around $\sqrt{s_{\mathrm{NN}}}$ = 27 GeV. Concurrently, measurements by the NA61/SHINE experiment present a different picture: no significant intermittency signal (i.e., no rise in the second-order SFM) was found for protons in Ar+Sc collisions at $\sqrt{s_{\mathrm{NN}}}$ = 5.1, 6.1, 7.6, 8.8, 11.9, and 16.8 GeV [21], while an increasing trend in the second-order correlator SFM was observed for negatively charged hadrons in central Xe+La collisions at $\sqrt{s_{\mathrm{NN}}}$ = 16.8 GeV [26]. These findings thus underscore two critical open questions: how do non-critical backgrounds specifically affect the intermittency measurements, particularly the non-critical baseline, and what is the possible fraction of critical signal in current experimental data?

In this paper, we address these open questions by employing the ultrarelativistic quantum molecular dynamics (UrQMD) model to systematically evaluate the non-critical background contributions to intermittency observables—specifically, the scaled factorial moments and the associated scaling index. The UrQMD model [27–31] incorporates essential non-critical dynamics of heavy-ion collisions, including energy–momentum and charge conservation, resonance decay, hadronic rescattering, collective flow and so on, while it does not incorporate any critical density fluctuations driven by the QCD phase transition. It therefore serves as an ideal tool for quantifying background effects. To establish a clean reference that removes all inherent correlations in the UrQMD data, we also analyze stochastic Gaussian samples whose transverse momenta of the particles in an event are Gaussian random variables. Furthermore, to estimate the precise fraction of critical signal present in the experimental data, we implement a hybrid UrQMD+CMC framework, in which density fluctuations with fractal criticality—generated via the critical Monte Carlo (CMC) model—are embedded into the transverse momentum spectra of particles from UrQMD events. Unlike previous analyses [32,33], which investigated on the scaling index whose physical interpretation remains debated, we perform a direct,

quantitative comparison between the SFMs obtained from the UrQMD+CMC model and those reported by the STAR experiment. This comprehensive approach allows us to disentangle critical and non-critical contributions, thereby offering clearer insight into the nature of the observed intermittency.

The paper is structured as follows. In Section 2, we introduce the framework of intermittency analysis using scaled factorial moments. Section 3 describes the cascade UrQMD model and presents the directly calculated SFMs for charged hadrons including protons (p), antiprotons ($\bar{p}$), kaons ($K^{\pm}$), and pions ($\pi^{\pm}$) together, in Au+Au collisions at $\sqrt{s_{\rm NN}} = 7.7$–200 GeV. Following this, Section 4 details the use of a Gaussian distribution to simulate the background and shows the corresponding SFM results. The highlight of this study is presented in Section 5, where we describe the hybrid UrQMD+CMC model and employ it to extract the precise critical signal from the STAR data. Finally, a summary and outlook are provided in Section 6.

2. Intermittency Analysis Method

Intermittency in the heavy-ion collision system can be measured through the scaled factorial moments (SFMs), namely $F_q(M)$, of particle multiplicity distributions in phase space. The factorial moment is defined as [18,20,22,34–36]

$$F_q(M) = \frac{\langle \frac{1}{M^D} \sum_{i=1}^{M^D} n_i(n_i-1)\cdots(n_i-q+1)\rangle}{\langle \frac{1}{M^D} \sum_{i=1}^{M^D} n_i\rangle^q}, \tag{1}$$

where q is the order of the factorial moment, D is the dimension of the phase space, and each dimension of phase space is divided into M equal bins, so that the total number of cells is M^D. Here, n_i denotes the particle multiplicity in the i-th cell, and $\langle\cdots\rangle$ represents the average over all events.

If the collision system exhibits intermittency, $F_q(M)$ are expected to follow a power-law (scaling) relation with M^2, known as the $F_q(M)/M$ scaling [18,19,22,23,37]:

$$F_q(M) \propto (M^D)^{\phi_q}, \quad M \gg 1, \tag{2}$$

where ϕ_q is the intermittency index. A larger value of ϕ_q indicates stronger intermittency. According to 3D Ising-QCD theory, if a system freezes out close to the critical point, the critical intermittency index is predicted to be $\phi_q = \frac{5\times(q-1)}{6}$ for protons (p) [18] and $\phi_q = \frac{2\times(q-1)}{3}$ for pions (π) [20,37].

Furthermore, if intermittency is present, the factorial moments also exhibit another scaling behavior: a power-law relation between the higher-order moment $F_q(M)$ and the second-order moment $F_2(M)$, known as the $F_q(M)/F_2(M)$ scaling [34,38–42]:

$$F_q(M) \propto F_2(M)^{\beta_q}, \quad M \gg 1, \tag{3}$$

where $\beta_q = \phi_q/\phi_2$ is the scaling coefficient. As described by Ginzburg-Landau theory for phase transitions [34,38], the $F_q(M)/M$ scaling behavior (Equation (2)) can be weakened or even washed out during the evolution of the system, because ϕ_q depends on specific critical parameters that are unknown and vary with the temperature of the evolving system. In contrast, β_q is independent of these specific critical parameters. Consequently, the $F_q(M)/F_2(M)$ scaling (Equation (3)) is expected to survive the dynamical evolution and can be measured experimentally.

Importantly, the scaling exponent ν, which characterizes the $F_q(M)/F_2(M)$ scaling across different orders, quantifies the strength of intermittency [34,38,39,42,43]:

$$\beta_q \propto (q-1)^{\nu}. \tag{4}$$

Ginzburg-Landau theory predicts a critical value of $\nu = 1.30$ for a system near the QCD critical point [34], while the two-dimensional Ising model predicts a value of 1.0 [38,44]. It should be noted that these predictions refer to the full phase space, whereas experimental measurements are limited to finite acceptances. Since both the intermittency index (ϕ_q) and the scaling exponent (ν) reflect the strength of intermittency in heavy-ion collisions, their dependence on collision energy may be used to locate the QCD critical point.

Collision systems typically have significant background effects—such as conservation laws, Coulomb repulsion, resonance decay, and finite detector acceptance—which can easily overwhelm the weak critical intermittency signal remaining in the final state of heavy-ion collisions. To remove these background contributions at the level of SFMs, a correlator moment $\Delta F_q(M)$ is introduced, defined as the difference between the SFMs computed from the original data and those from corresponding mixed events [22–24,45]:

$$\Delta F_q(M) = F_q(M)^{\text{data}} - F_q(M)^{\text{mix}}. \tag{5}$$

Here, the mixed-event sample is strictly constructed by randomly selecting particles from the original dataset, with each particle in a given mixed event drawn from a different original event, while ensuring that the mixed events have the same multiplicity and momentum distributions as the original events.

3. Intermittency of Charged Hadrons from the Cascade UrQMD Model

The UrQMD model [27–31,46] is a well-established transport approach widely employed to simulate dynamical evolution of high-energy collisions—including $p+p$, $p+A$, and $A+A$ systems—across energies ranging from a few GeV up to the TeV scale attained at the CERN-LHC. In this model, all hadrons are propagated according to Hamilton's equations of motion and interact via stochastic binary scatterings, the excitation and fragmentation of color strings, and decay of hadronic resonances [27,46]. As it incorporates essential non-critical dynamics of heavy-ion collisions and does not include the physical regime of the QCD phase transition, UrQMD provides a suitable baseline for estimating non-critical contributions. In this work, the cascade mode of UrQMD (version 3.4) is employed to generate event samples for Au+Au collisions at RHIC energies. The generated event statistics are 3.96, 8.80, 18.0, 35.4, 1.20, 1.30, and 1.0×10^6 at $\sqrt{s_{\text{NN}}} = 7.7$, 11.5, 19.6, 27, 39, 62.4, and 200 GeV, respectively.

The analysis framework adopted in this study follows that used in the STAR experiment, encompassing centrality definition, kinematic selections, analysis acceptance, fitting procedures, and related methodologies [24,25]. Charged hadrons—specifically protons (p), antiprotons ($\bar{p}$), kaons ($K^{\pm}$), and pions ($\pi^{\pm}$)—are selected within the pseudorapidity interval $|\eta| < 0.5$. The applied transverse momentum (p_T) ranges are $0.2 < p_T < 1.6$ GeV/c for $K^{\pm}$ and $\pi^{\pm}$, and $0.4 < p_T < 2.0$ GeV/c for p and $\bar{p}$. To avoid autocorrelation effects, the collision centrality is determined using uncorrected charged-particle multiplicities in the pseudorapidity region $0.5 < |\eta| < 1.0$, which lies outside the analysis window $|\eta| < 0.5$. The two-dimensional transverse-momentum space, $[-2.0 < p_x < 2.0\text{GeV}/c] \otimes [-2.0 < p_y < 2.0\text{GeV}/c]$, is subdivided into M^2 equal-area cells, with M^2 varied from 1 to 100^2, for the calculation of $F_q(M)$.

In the upper panels of Figure 1, we present the factorial moments $F_q(M)$ for charged hadrons from UrQMD simulations (red solid symbols) and the corresponding mixed events

(black open symbols) as a function of M^2 in the most central (0–5%) Au+Au collisions at $\sqrt{s_{\rm NN}}$ = 7.7, 27, 39, and 200 GeV. The UrQMD results show a gradual increase in $F_q(M)$ with M^2, saturating for $M^2 > 1000$. Furthermore, all measured orders ($q = 2-6$) of $F_q(M)^{\rm UrQMD}$ are overlapped with $F_q(M)^{\rm mix}$ across all collision energies, indicating that the magnitude of $F_q(M)$ in UrQMD simulations arises from non-critical dynamical processes inherent to the cascade model.

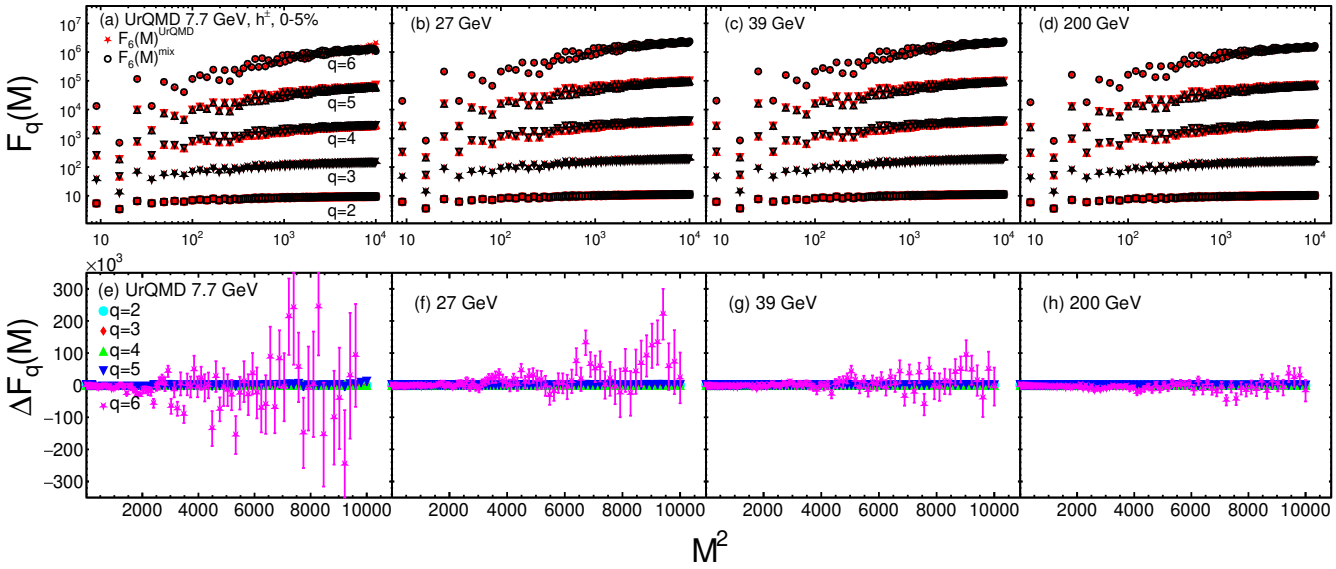

Figure 1. (**a**–**d**) Scaled factorial moments $F_q(M)$ of data and corresponding mixed events (up to sixth order), as a function of the number of cells (M^2) for charged hadrons in the most central (0–5%) Au+Au collisions at $\sqrt{s_{\rm NN}}$ = 7.7–200 GeV from the UrQMD model, plotted on a double-logarithmic scale. Results from the original data and the corresponding mixed events are shown in red solid and black open markers, respectively. (**e**–**h**) The correlator moment $\Delta F_q(M)$, calculated using Equation (5), as a function of M^2. Statistical uncertainties are evaluated via the Bootstrap method.

By using the mixed events to remove the background contribution, the corrected moment $\Delta F_q(M)$, calculated via Equation (5), are displayed in the lower panels of Figure 1. The values of $\Delta F_q(M)$ are found to be consistent with zero within statistical uncertainties. This observation aligns with the absence of any rise in the SFMs, which is expected because the UrQMD model does not incorporate density fluctuations associated with the QCD phase transition. These results also confirm the suitability of the mixed-event method for background removal in such analyses.

In the STAR experiment, a strict power-law dependence of $\Delta F_q(M)$ ($q = 3$–6) on $\Delta F_2(M)$—referred to as $\Delta F_q(M)/\Delta F_2(M)$ scaling—has been observed in the most central (0–5%) Au+Au collisions [24]. In this study, we examine the corresponding behavior for $h^{\pm}$ from the UrQMD model without background subtraction. Figure 2 shows $F_q(M)$ ($q = 3$–6) as a function of $F_2(M)$. A power-law scaling of $F_q(M)$ is also evident in the UrQMD results, demonstrating that non-critical dynamics alone can produce such a scaling pattern among the factorial moments. It is noteworthy that this scaling disappears when the background contributions, estimated via the mixed-event method, are subtracted from the UrQMD data. The values of the exponent β_q, extracted by fitting $F_q(M)$ with Equation (3), are displayed adjacent to the corresponding fit lines in Figure 2.

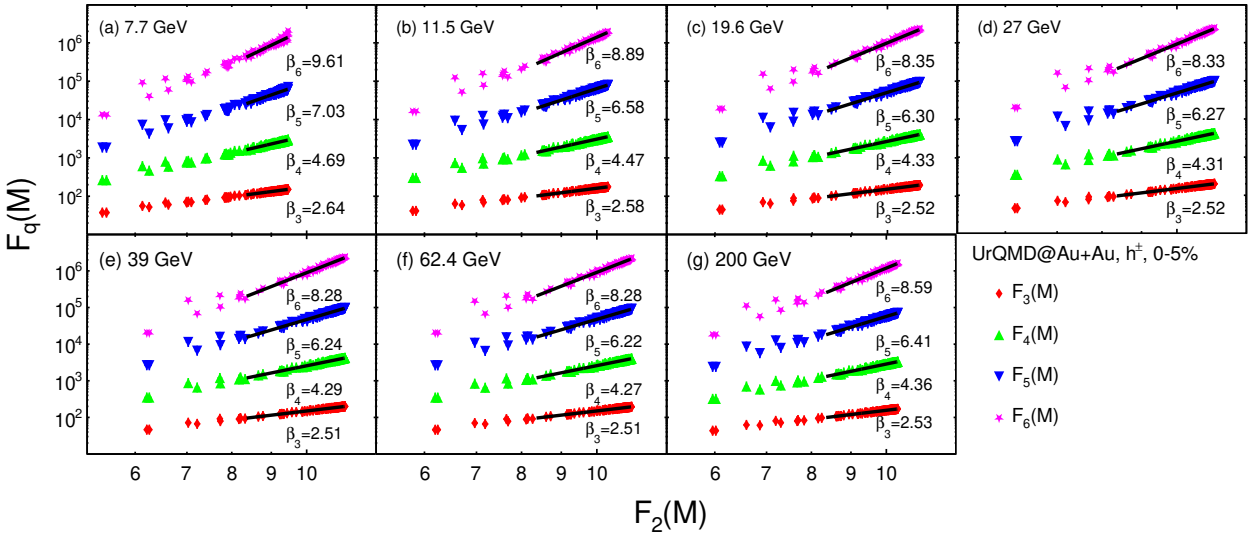

Figure 2. Higher-order scaled factorial moments $F_q(M)$ (q = 3–6) as a function of the second-order moment $F_2(M)$ for charged hadrons produced in the most central (0–5%) Au+Au collisions at $\sqrt{s_{\rm NN}}$ = 7.7–200 GeV from the UrQMD model. The black solid line represents a power-law fit $F_q(M) \propto F_2(M)^{\beta_q}$ within the range $M \in [30, 100]$. The extracted exponent β_q for each order is indicated next to the corresponding fit line.

The scaling exponent ν is extracted by fitting β_q via Equation (4) for charged hadrons in the most central (0–5%) Au+Au collisions at $\sqrt{s_{\rm NN}}$ = 7.7–200 GeV from the UrQMD calculations without background subtraction, as shown in the upper panel of Figure 3. On the other hand, the lower panel displays the corresponding result from the STAR experiment, in which background contributions have been subtracted. It is important to note that the values of ν obtained from the UrQMD model are directly calculated from the scaling of $F_q(M)/F_2(M)$, without applying background subtraction via Equation (5). Therefore, the magnitude of ν in UrQMD reflects purely non-critical dynamical contributions, serving as a baseline for hadronic transport. In contrast, the ν values extracted from STAR data are obtained from the scaling of $\Delta F_q(M)/\Delta F_2(M)$, where $\Delta F_q(M)$ represents the factorial moment after subtracting the mixed-event background. It is found that the range of ν values from the UrQMD calculations is much larger than that from the STAR data, indicating that non-critical dynamics alone can yield a large ν.

The ν values from UrQMD are smaller than those reported from models such as AMPT (ν = 1.94) [42] and HIJING (ν = 1.824) [43]. The differences in ν obtained from various models arise from their distinct dynamical descriptions of the collision evolution. Additionally, variations in kinematic acceptance (e.g., η and p_T) and in the selection of analyzed particle species contribute to the observed discrepancies. Since none of these models include the critical fluctuations of the QCD phase transition, a larger ν value does not necessarily imply stronger fluctuations, as noted in earlier literature [38].

Regarding the collision energy dependence of ν, a distinct difference is observed. The UrQMD results show a monotonically decreasing trend of ν with increasing $\sqrt{s_{\rm NN}}$. In contrast, the STAR data exhibit a non-monotonic trend in energy dependence with a minimum around $\sqrt{s_{\rm NN}}$ = 27 GeV. This marked discrepancy suggests the presence of genuine dynamical density fluctuations in the heavy-ion collision system beyond those accounted by non-critical models. A full understanding of the experimental observations will therefore require dynamical models that incorporate the critical point. Finally, we note that in the UrQMD model, ν effectively vanishes when mixed-event method is used to subtract the background, because $\Delta F_q(M)$ is consistent with zero and accordingly the power-law scaling of $\Delta F_q(M) \propto \Delta F_2(M)^{\beta_q}$ is absent.

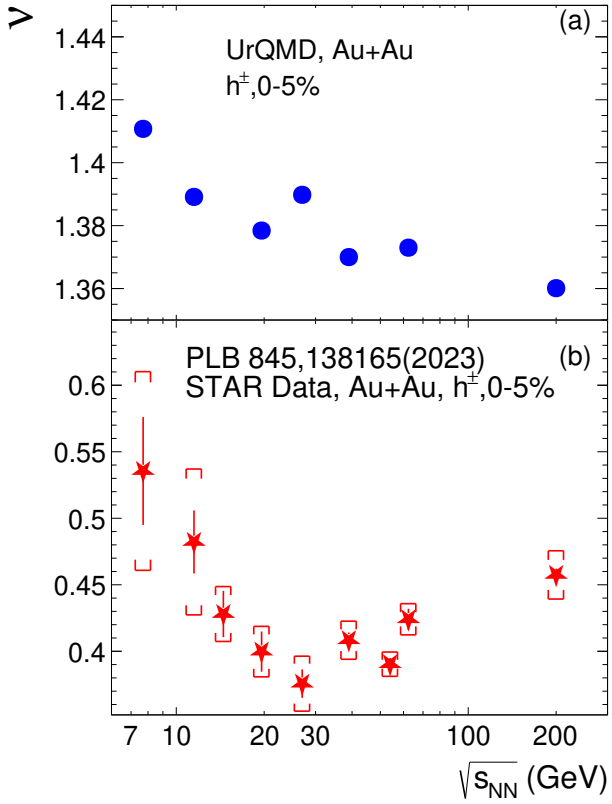

Figure 3. (**a**) Scaling exponent ν as a function of collision energy for charged hadrons ($h^{\pm}$) in the most central (0–5%) Au+Au collisions at $\sqrt{s_{\rm NN}} = 7.7$–200 GeV, obtained from the UrQMD model without background subtraction. (**b**) Energy dependence of ν from the STAR experiment after background subtraction via the mixed-event method, taken from Ref. [24].

4. SFMs from the Gaussian Sample

As shown in the previous section, non-critical dynamical fluctuations can contribute to the observed $F_q(M)$ and ν values. Therefore, a clean baseline that removes all inherent correlations present in the UrQMD data is required. For this purpose, we generate a synthetic data set by sampling particle momenta from a Gaussian distribution. A total of 1 million events are produced. The charged-particle multiplicity per event is sampled from a Poisson distribution with a mean value of $\langle N_{\rm ch} \rangle = 150$, chosen to be close to the measured value of 151 at $\sqrt{s_{\rm NN}} = 19.6$ GeV in the STAR experiment. Within each event, the transverse momenta (p_x, p_y) of particles are generated as Gaussian random variables with a mean of zero and a variance of $\sigma = 0.5$. An additional cut of $p_T < 2.0$ GeV/c is applied to this Gaussian data set.

The same analysis procedure is applied to the Gaussian data set, with the results presented in Figure 4. Figure 4a displays the p_x-p_y distribution of particles in the Gaussian sample. Figure 4b shows $F_q(M)^{\rm data}$ and $F_q(M)^{\rm mix}$ as functions of M^2, while Figure 4c presents the corresponding $\Delta F_q(M)$ versus M^2. Similar to the findings from the UrQMD model, $F_q(M)^{\rm data}$ is overlapped with $F_q(M)^{\rm mix}$ across all moments, and the values of $\Delta F_q(M)$ are compatible with zero within statistical uncertainties. This result, however, differs from that reported in Ref. [47], where $\Delta F_q(M)$ was found to be significantly positive and followed the $\Delta F_q(M)/\Delta F_2(M)$ scaling. The discrepancy can be attributed primarily to the much larger mean multiplicity ($\langle N_{\rm ch} \rangle = 10,000$) and a different implementation of the mixed-event method used in the referenced study [47].

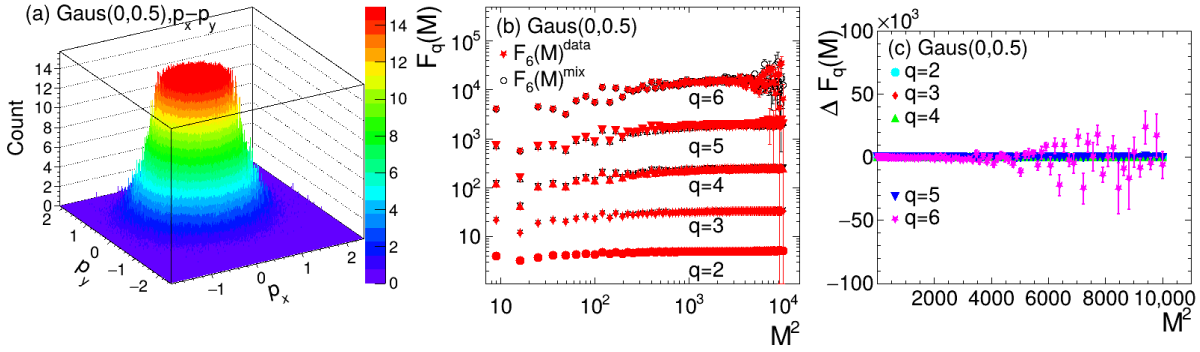

Figure 4. (**a**) Transverse momentum (p_x-p_y) distribution for Gaussian-sampled data. (**b**) $F_q(M)$ (q = 2–6) as a function of M^2, comparing original data and corresponding mixed events from Gaussian sample. (**c**) Corresponding correlator moment $\Delta F_q(M)$ plotted versus M^2.

5. Quantifying the Critical Signal in STAR Data with Hybrid UrQMD+CMC Model

Current UrQMD calculations show no indication of intermittency signal in Au+Au collisions at RHIC energies. To date, a model capable of simulating critical intermittency driven by local density fluctuations near the QCD critical point is the critical Monte Carlo (CMC) model [18,20,32,33,48]. This model generates particle momenta via Lévy random walks, thereby creating localized, critical density fluctuations in momentum space. It should be noted that the CMC is essentially a toy model, designed as a static momentum space generator rather than a dynamical simulation. It only supplies momentum space distributions for final-state particles and does not include any dynamical evolution of the collision system, unlike transport models such as UrQMD which simulate the full heavy-ion collision process including nonequilibrium transport description and hadronic evolution.

To reproduce the intermittency signal observed by the STAR experiment—specifically, the rise of $\Delta F_q(M)$ with M^2 and the distinct $\Delta F_q(M)/\Delta F_2(M)$ scaling—we combine the UrQMD and CMC models into a hybrid UrQMD+CMC framework. The combination method robustly introduces CMC particles, whose momentum profiles contain critical fluctuations, into the final-state particles yield from UrQMD events, which provide the dynamical background.

A key parameter is the critical particle fraction, defined by the replacement ratio $\alpha_{\text{particle}} = N_{\text{CMC}}/N_{\text{UrQMD}}$. Here, N_{CMC} is the number of selected CMC particles added to a pure UrQMD event, and N_{UrQMD} is the number of charged hadrons in that background UrQMD event. A larger α_{particle} corresponds to a greater number of CMC particles carrying the critical signal, which leads to a stronger critical signature superimposed on the non-critical UrQMD background. Physically, α_{particle} represents the fraction of critical particles whose primordial critical information remains detectable and is not obscured by substantial background effects and dynamical noise throughout the evolution of a heavy-ion collision.

The procedure for generating UrQMD+CMC events is as follows:

1. Generate a sample of UrQMD events with the desired collision parameters, recording the charged-particle multiplicity N_{ch} and momenta for each event.
2. Configure the CMC model with the Lévy parameter $\mu = 1/6$ and $p_{\text{min}}/p_{\text{max}} = 10^{-7}$, corresponding to a critical system in the 3D Ising universality class with a fractal dimension $d_F = 1/3$ [18,48]. This choice ensures the resulting intermittency indices from CMC calculations are consistent with theoretical predictions. Then, a particle with $p_T < 0.5$ GeV/c from the UrQMD event is randomly selected to serve as the

seed for a Lévy random walk. This walk generates a sequence of particle momenta, constituting a CMC event. The CMC event is required to have the same N_{ch} and a similar transverse momentum spectrum as the associated UrQMD event.

3. Perform particle replacement: Randomly select one particle from the UrQMD event and one from the matched CMC event. Replace the UrQMD particle with the CMC particle if the condition $|p_T^{\mathrm{CMC}} - p_T^{\mathrm{UrQMD}}| < 0.2$ GeV/c is satisfied. If this condition is not met, the random selection is repeated until a suitable pair is found. Once a replacement is made, the used CMC particle is removed from the CMC dataset. The p_T-matching criterion preserves the global p_T spectrum of the original UrQMD events in the final hybrid sample.
4. Repeat step 3 until the number of replaced particles reaches the target value defined by $\alpha_{\mathrm{particle}}$. The remaining UrQMD particles and the newly coming CMC particles together constitute a single UrQMD+CMC event.
5. Apply steps 2–4 to all UrQMD events in the sample to produce the complete hybrid dataset.

Figure 5 presents results from the hybrid UrQMD+CMC model. Figure 5a shows the pattern of critical intermittency from the pure CMC model (i.e., 100% critical signal). A clear power-law dependence of $F_q(M)$ on M^2 is observed, with $F_q(M)^{\mathrm{data}}$ significantly exceeding $F_q(M)^{\mathrm{mix}}$, particularly for higher-order moments ($q = 5$–6). Figure 5b displays $F_q(M)^{\mathrm{data}}$ and $F_q(M)^{\mathrm{mix}}$ ($q = 2$–6) versus M^2 for the UrQMD+CMC model with a small critical particle fraction, $\alpha_{\mathrm{particle}} = 1.8\%$. Here, $F_q(M)^{\mathrm{data}}$ is slightly larger than $F_q(M)^{\mathrm{mix}}$, indicating a weak critical signal superimposed on the UrQMD background. This behavior closely resembles the trend observed in the STAR experimental data. The corresponding $\Delta F_q(M)$ are shown in Figure 5c. While $\Delta F_q(M)$ broadly follows a power-law increase with M^2, distortions become apparent at higher orders ($q = 5$–6). Despite the small critical fraction, the second-order moment $\Delta F_2(M)$ remains largely unaffected, yielding an extracted intermittency index $\phi_2 = 0.70 \pm 0.1$. This value is close to the critical prediction of 0.67, suggesting that $\Delta F_2(M)$ can be used as a particularly suitable observable to extract weak signals of critical intermittency by comparing UrQMD+CMC simulations with STAR data. Finally, Figure 5d shows the scaling of $\Delta F_q(M)$ with $\Delta F_2(M)$. The $\Delta F_q(M)/\Delta F_2(M)$ scaling relation holds reasonably well across the measured orders, although a deviation is visible for $q = 6$. Notably, this deviation is smaller than that observed in the $\Delta F_6(M)/M$ scaling in Figure 5b, indicating the relative stability of the $\Delta F_q(M)/\Delta F_2(M)$ scaling approach.

In previous studies [32,33], the ν calculated from the UrQMD+CMC model was compared with corresponding measurements from the STAR experiment. It was found that the model calculation of ν agrees with the experimental data when an intermittency signal of about 1–2% is introduced into the UrQMD sample. However, the physical interpretation of ν remains debated. In particular, its expected critical value—accounting for a realistic reduced transverse-momentum phase space and detector acceptance—has not yet been established. More importantly, as noted in the preceding paragraph, higher-order moments $\Delta F_q(M)$ become distorted at small $\alpha_{\mathrm{particle}}$. Since ν is derived from these higher-order moments, its extracted value can be significantly affected by such distortions, making a direct comparison between model and experiment less conclusive.

To circumvent this difficulty, we perform a direct, quantitative comparison using the second-order moment $\Delta F_2(M)$. This observable remains largely unaffected even for small values of $\alpha_{\mathrm{particle}}$ and its physical interpretation is well established. In Figure 6, we compare $\Delta F_2(M)$ between UrQMD+CMC simulations and STAR data at $\sqrt{s_{\mathrm{NN}}}$ = 7.7, 11.5, 19.6, and 27 GeV. The experimental data (red stars) lie systematically between the model calculations for $\alpha_{\mathrm{particle}} = 1.5\%$ and 2.2%, and are nearly consistent with the simulation using $\alpha_{\mathrm{particle}} = 1.8\%$. This close agreement allows us to draw a well-supported conclusion:

a critical intermittency signal on the order of approximately 1.8% could be present in the most central Au+Au collisions reported by the STAR experiment.

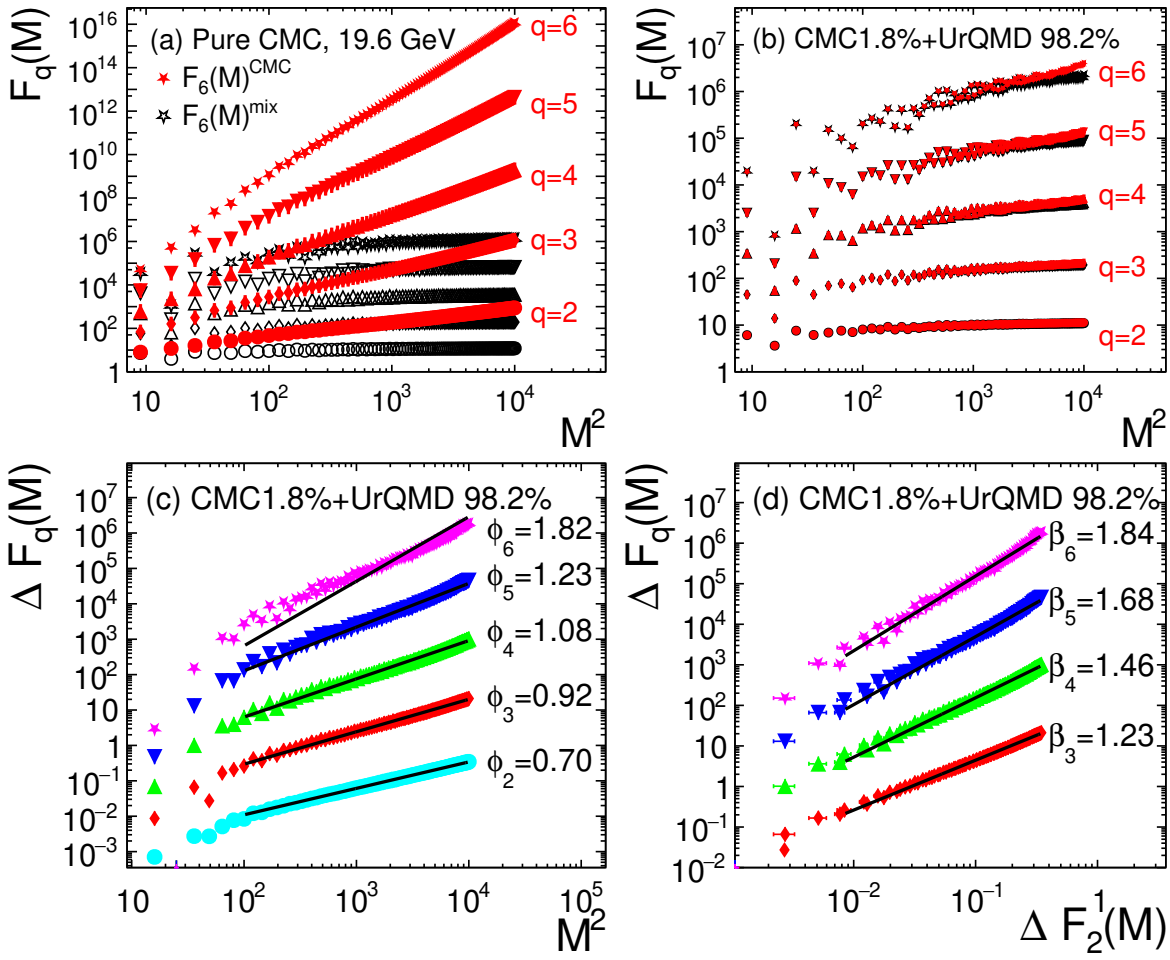

Figure 5. (**a**) Scaled factorial moments $F_q(M)^{\text{data}}$ and $F_q(M)^{\text{mix}}$ (q = 2–6) as a function of M^2, obtained from the pure (100% critical signal) CMC model. (**b**) $F_q(M)^{\text{data}}$ and $F_q(M)^{\text{mix}}$ as a function of M^2, from the UrQMD+CMC model with a critical particle fraction $\alpha_{\text{particle}} = 1.8\%$. (**c**) Corresponding correlator $\Delta F_q(M)$ versus M^2. (**d**) Corresponding correlator $\Delta F_q(M)$ versus $\Delta F_2(M)$. The extracted exponents ϕ_q and β_q for each order are indicated beside the corresponding fit lines.

The $\Delta F_2(M)$ obtained from the hybrid model exhibits a linear dependence on M^2 across the entire M^2 range. In contrast, the corresponding experimental data from STAR show an upward curvature, eventually saturating at larger M^2. This discrepancy may arise from the effect of dimensional reduction present in the experimental data, which is not accounted for in the current CMC simulation. As noted in earlier studies [49,50], critical local fluctuations are expected to be self-affine rather than strictly self-similar. Consequently, while a clear power-law scaling of $F_q(M)$ exists in the full three-dimensional momentum space, its projection onto the two-dimensional p_x-p_y plane—analyzed under the assumption of self-similarity—can yield a curved rather than a purely linear dependence. We therefore emphasize that the extracted critical fraction of approximately 1.8% is inherently model-dependent. An improved CMC model that includes a self-affine structure for the critical component may better describe the observed curvature in $\Delta F_2(M)$ and thus lead to a revised estimate. Future studies need to incorporate self-affine scaling into such analyses in order to achieve a more precise and well-founded quantification of the critical signal fraction.

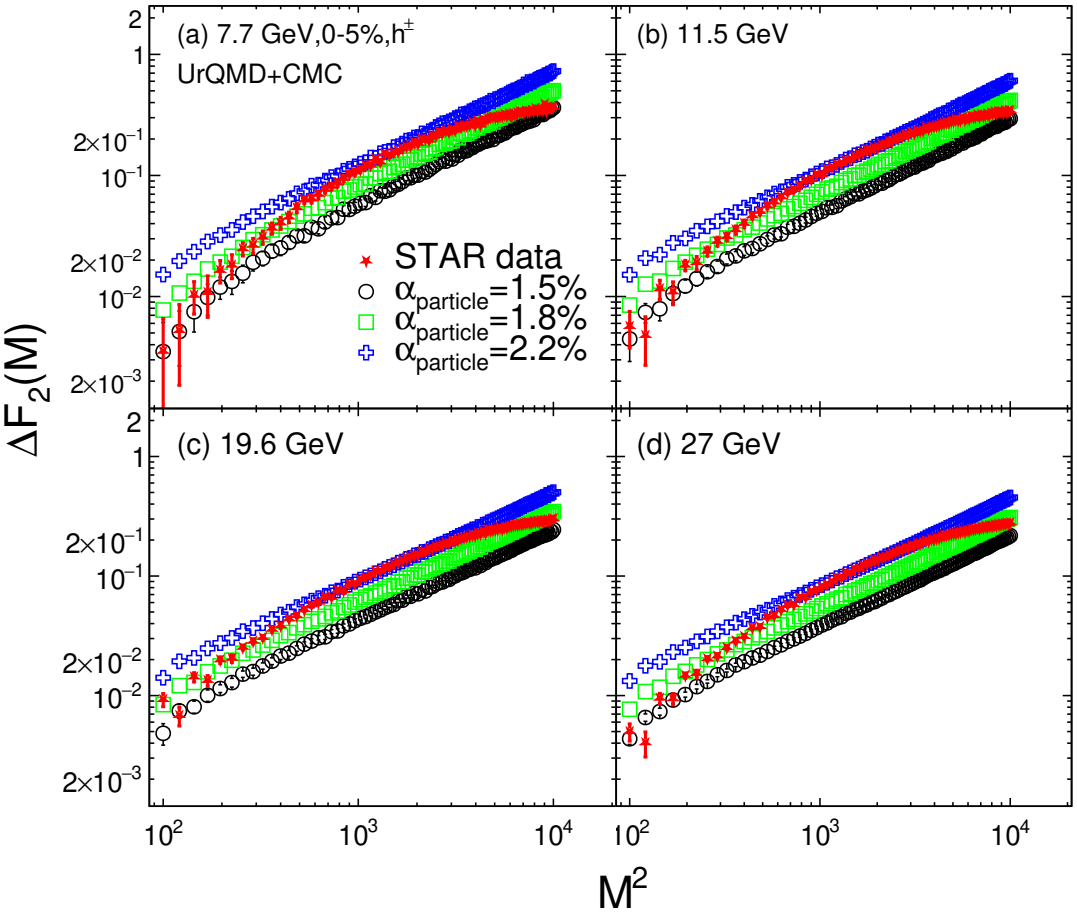

Figure 6. The second-order correlator $\Delta F_2(M)$ as a function of M^2 at $\sqrt{s_{\rm NN}}$ = 7.7, 11.5, 19.6, and 27 GeV. The red stars represent $\Delta F_2(M)$ from the STAR experiment, while the open symbols correspond to results from the UrQMD+CMC model with critical particle fractions $\alpha_{\rm particle}$ = 1.5%, 1.8%, and 2.2%, respectively.

6. Summary and Outlook

In summary, we have performed a systematic model study to investigate the intermittency signal in Au+Au collisions at RHIC energies, with the aim of assessing non-critical background contributions and quantifying the fraction of critical signal present in experimental data. Using the UrQMD cascade model, which incorporates essential non-critical dynamics but no density fluctuations of the QCD phase transition, we first established that non-critical processes alone can produce sizable $F_q(M)$ and yield a large ν. Notably, without background subtraction, UrQMD shows a monotonically decreasing trend of ν with increasing $\sqrt{s_{\rm NN}}$, in clear contrast to the non-monotonic energy dependence with a minimum near $\sqrt{s_{\rm NN}} = 27$ GeV observed in the background-subtracted STAR data. Crucially, these background-induced signals vanish when the mixed-event subtraction is applied, yielding $\Delta F_q(M)$ consistent with zero. This confirms both the necessity and the effectiveness of background subtraction in intermittency analyses and highlights the risk of misinterpreting non-critical correlations as critical phenomena if such subtraction is omitted.

To probe the critical signal in the experimental data, we developed a hybrid UrQMD+CMC framework, in which critical density fluctuations generated by the CMC model are embedded into the UrQMD hadronic background. Moving beyond previous comparisons that relied on the exponent ν—which carries theoretical uncertainties and is sensitive to distortions in higher-order moments at small critical fraction—we advocated for a more particularly suitable

observable: the second-order moment $\Delta F_2(M)$. This quantity remains stable even for weak critical signals and has a clearer physical interpretation. Our central quantitative result is that the $\Delta F_2(M)$ measured by STAR in the most central Au+Au collisions at $\sqrt{s_{\mathrm{NN}}} = 7.7$–$27$ GeV systematically lies between the calculations of the UrQMD+CMC model with critical particle fractions $\alpha_{\mathrm{particle}} = 1.5\%$ and 2.2%, showing excellent agreement with the model curve for $\alpha_{\mathrm{particle}} = 1.8\%$. This allows us to estimate that a critical intermittency signal on the order of approximately 1.8% could be present in the experimental data.

Looking forward, several refinements and extensions can deepen this analysis. A primary limitation is the model dependence of the extracted critical fraction. This may arise from the fact that the current CMC implementation assumes self-similar critical fluctuations, whereas theory and earlier studies indicate they should be self-affine in three-dimensional momentum space. The observed discrepancy in the shape of $\Delta F_2(M)$ versus M^2—linear in the model but curved in the data—likely originates from this simplification. Future implementations should incorporate self-affine scaling to better model the projection from the full momentum space onto the analyzed two-dimensional transverse-momentum plane. Second, beyond the particle-level replacement (parameterized by $\alpha_{\mathrm{particle}}$) studied here, an event-level admixture scheme should be explored. This would correspond to a physical scenario in which only a subset of heavy-ion collisions traverse the critical region of the QCD phase diagram, providing a more realistic mapping between the critical fraction and collision dynamics. Third, our hybrid approach introduces critical signals statically into the final state of the UrQMD simulation. A more complete treatment requires dynamically coupling the evolution of critical modes with the hadronic transport, which would provide a more realistic description of the space-time development of fluctuations.

In conclusion, this study underscores the significant role of non-critical backgrounds in intermittency observables and demonstrates a practical methodology to disentangle them from potential critical signal. The estimated critical signal fraction of approximately 1.8% provides a quantitative benchmark for interpreting current STAR results and offers valuable guidance for ongoing and future experiments in the search for the QCD critical point.

Author Contributions: Conceptualization, J.W. and Z.L.; Methodology, Z.L.; Software, J.W. and S.L.; Validation, S.L.; Formal analysis, J.W.; Investigation, Z.L.; Resources, S.L.; Data curation, J.W.; Writing—original draft, J.W.; Writing—review & editing, J.W. and Z.L.; Visualization, S.L.; Supervision, Z.L.; Project administration, Z.L.; Funding acquisition, J.W., Z.L. and S.L. All authors have read and agreed to the published version of the manuscript.

Funding: This work is supported by Guangxi Natural Science Foundation under Grant No. 2025GXNSFBA069070, Basic Ability Enhancement Project of University Education in Guangxi for Young Teachers' Research (No. 2024KY0282), the National Natural Science Foundation of China (No. 12275102), and the Natural Science Foundation of Henan under contract No. 252300420921.

Data Availability Statement: The original contributions presented in this study are included in the article. Further inquiries can be directed to the corresponding author.

Conflicts of Interest: The authors declare no conflicts of interest.

References

1. Bzdak, A.; Esumi, S.; Koch, V.; Liao, J.; Stephanov, M.; Xu, N. Mapping the Phases of Quantum Chromodynamics with Beam Energy Scan. *Phys. Rept.* **2020**, *853*, 1–87. [CrossRef]
2. Braun-Munzinger, P.; Stachel, J. The quest for the quark-gluon plasma. *Nature* **2007**, *448*, 302–309. [CrossRef]
3. Aboona, B.E.; Adam, J.; Adamczyk, L.; Aggarwal, I.; Aggarwal, M.M.; Ahammed, Z.; Alshammri, A.K.; Aschenauer, E.C.; Aslam, S.; Atchison, J.; et al. Precision Measurement of Net-Proton-Number Fluctuations in Au+Au Collisions at RHIC. *Phys. Rev. Lett.* **2025**, *135*, 142301. [CrossRef]

4. Abdallah, M.S.; Aboona, B.E.; Adam, J.; Adamczyk, L.; Adams, J.R.; Adkins, J.K.; Agakishiev, G.; Aggarwal, I.; Aggarwal, M.M.; Ahammed, Z.; et al. Measurements of Proton High Order Cumulants in $\sqrt{s_{NN}}$ = 3 GeV Au+Au Collisions and Implications for the QCD Critical Point. *Phys. Rev. Lett.* **2022**, *128*, 202303. [CrossRef]
5. Luo, X.; Xu, N. Search for the QCD Critical Point with Fluctuations of Conserved Quantities in Relativistic Heavy-Ion Collisions at RHIC: An Overview. *Nucl. Sci. Tech.* **2017**, *28*, 112. [CrossRef]
6. Zhang, Y.; Zhang, D.; Luo, X. Experimental study of the QCD phase diagram in relativistic heavy-ion collisions. *Nucl. Tech.* **2023**, *46*, 4. [CrossRef]
7. Luo, X.; Wang, Q.; Xu, N.; Zhuang, P. (Eds.) *Properties of QCD Matter at High Baryon Density*; Springer: Berlin/Heidelberg, Germany, 2022. [CrossRef]
8. Aoki, Y.; Endrődi, G.; Fodor, Z.; Katz, S.D.; Szabo, K.K. The Order of the quantum chromodynamics transition predicted by the standard model of particle physics. *Nature* **2006**, *443*, 675–678. [CrossRef]
9. Ejiri, S. Canonical partition function and finite density phase transition in lattice QCD. *Phys. Rev. D* **2008**, *78*, 074507. [CrossRef]
10. Bowman, E.S.; Kapusta, J.I. Critical Points in the Linear Sigma Model with Quarks. *Phys. Rev. C* **2009**, *79*, 015202. [CrossRef]
11. Hatta, Y.; Stephanov, M.A. Proton number fluctuation as a signal of the QCD critical endpoint. *Phys. Rev. Lett.* **2003**, *91*, 102003. [CrossRef] [PubMed]
12. Tribedy, P. Highlights from the STAR Experiment. *Acta Phys. Polon. Supp.* **2023**, *16*, 1-A6. [CrossRef]
13. Maćkowiak-Pawłowska, M. NA61/SHINE results on fluctuations and correlations at CERN SPS energies. *Nucl. Phys. A* **2021**, *1005*, 121753. [CrossRef]
14. Adhikary, H.; Adrich, P.; Allison, K.K.; Amin, N.; Andronov, E.V.; Antićić, T.; Arsene, I.C.; Bajda, M.; Balkova, Y.; Baszczyk, M.; et al. Search for the critical point of strongly-interacting matter in ^{40}Ar + ^{45}Sc collisions at 150A GeV/c using scaled factorial moments of protons. *Eur. Phys. J. C* **2023**, *83*, 881. [CrossRef]
15. Guo, D.; Xu, H.; Qi, D.; Wang, H.; Huang, S.; Zhang, L.; Sun, Z.; Qin, Z.; Wang, B.; Zhou, Y.; et al. The trigger system for the HIRFL-CSR external-target experiment. *JINST* **2024**, *19*, T02018. [CrossRef]
16. Ablyazimov, T.; Abuhoza, A.; Adak, R.P.; Adamczyk, M.; Agarwal, K.; Aggarwal, M.M.; Ahammed, Z.; Ahmad, F.; Ahmad, N.; Ahmad, S.; et al. Challenges in QCD matter physics –The scientific programme of the Compressed Baryonic Matter experiment at FAIR. *Eur. Phys. J. A* **2017**, *53*, 60. [CrossRef]
17. Golovatyuk, V.; Kekelidze, V.; Kolesnikov, V.; Rogachevsky, O.; Sorin, A. Multi-Purpose Detector to study heavy-ion collisions at the NICA collider. *Nucl. Phys. A* **2019**, *982*, 963–966. [CrossRef]
18. Antoniou, N.G.; Diakonos, F.K.; Kapoyannis, A.S. Critical opalescence in baryonic QCD matter. *Phys. Rev. Lett.* **2006**, *97*, 032002. [CrossRef] [PubMed]
19. Antoniou, N.G.; Diakonos, F.K.; Maintas, X.N.; Tsagkarakis, C.E. Locating the QCD critical endpoint through finite-size scaling. *Phys. Rev. D* **2018**, *97*, 034015. [CrossRef]
20. Antoniou, N.G.; Contoyiannis, Y.F.; Diakonos, F.K.; Mavromanolakis, G. Critical QCD in nuclear collisions. *Nucl. Phys. A* **2005**, *761*, 149–161. [CrossRef]
21. Adhikary, H.; Adrich, P.; Allison, K.K.; Amin, N.; Andronov, E.V.; Antićić, T.; Arsene, I.C.; Bajda, M.; Balkova, Y.; Baszczyk, M.; et al. Search for a critical point of strongly-interacting matter in central ^{40}Ar + ^{45}Sc collisions at 13–75A GeV/c beam momentum. *Eur. Phys. J. C* **2024**, *84*, 741. [CrossRef]
22. Anticic, T.; Baatar, B.; Bartke, J.; Beck, H.; Betev, L.; Białkowska, H.; Blume, C.; Bogusz, M.; Boimska, B.; Book, J.; Botje, M. Critical fluctuations of the proton density in A+A collisions at 158A GeV. *Eur. Phys. J. C* **2015**, *75*, 587. [CrossRef]
23. Anticic, T.; Baatar, B.; Barna, D.; Bartke, J.; Betev, L.; Białkowska, H.; Blume, C.; Boimska, B.; Botje, M.; Bracinik, J.; et al. Search for the QCD critical point in nuclear collisions at the CERN SPS. *Phys. Rev. C* **2010**, *81*, 064907. [CrossRef]
24. Abdulhamid, M.I.; Aboona, B.E.; Adam, J.; Adamczyk, L.; Adams, J.R.; Aggarwal, I.; Aggarwal, M.M.; Ahammed, Z.; Anderson, D.M.; Aschenauer, E.C.; et al. Energy dependence of intermittency for charged hadrons in Au+Au collisions at RHIC. *Phys. Lett. B* **2023**, *845*, 138165. [CrossRef]
25. Wu, J.; Luo, X.; Li, Z.; Wu, Y. Overview of Recent Intermittency Analysis in Relativistic Heavy-ion Collisions. *Nucl. Phys. Rev.* **2024**, *41*, 580–586. [CrossRef]
26. Reyna Ortiz, V.Z. Search for the Critical Point via Intermittency Analysis in NA61/SHINE. *Ukr. J. Phys.* **2024**, *69*, 858. [CrossRef]
27. Bleicher, M.; Zabrodin, E.; Spieles, C.; Bass, S.A.; Ernst, C.; Soff, S.; Bravina, L.; Belkacem, M.; Weber, H.; Stöcker, H.; et al. Relativistic hadron hadron collisions in the ultrarelativistic quantum molecular dynamics model. *J. Phys. G* **1999**, *25*, 1859–1896. [CrossRef]
28. Bass, S.A.; Belkacem, M.; Bleicher, M.; Brandstetter, M.; Bravina, L.; Ernst, C.; Gerland, L.; Hofmann, M.; Hofmann, S.; Konopka, J.; et al. Microscopic models for ultrarelativistic heavy ion collisions. *Prog. Part. Nucl. Phys.* **1998**, *41*, 255–369. [CrossRef]
29. Petersen, H.; Steinheimer, J.; Burau, G.; Bleicher, M.; Stöcker, H. A Fully Integrated Transport Approach to Heavy Ion Reactions with an Intermediate Hydrodynamic Stage. *Phys. Rev. C* **2008**, *78*, 044901. [CrossRef]

30. Bratkovskaya, E.L.; Bleicher, M.; Reiter, M.; Soff, S.; Stoecker, H.; van Leeuwen, M.; Bass, S.A.; Cassing, W. Strangeness dynamics and transverse pressure in relativistic nucleus-nucleus collisions. *Phys. Rev. C* **2004**, *69*, 054907. [CrossRef]
31. Bleicher, M.J.; Bass, S.A.; Bravina, L.V.; Greiner, W.; Soff, S.; Stoecker, H.; Xu, N.; Zabrodin, E.E. Global observables and secondary interactions in central Au + Au reactions at $\sqrt{s_{\mathrm{NN}}}$ = 200 GeV/A. *Phys. Rev. C* **2000**, *62*, 024904. [CrossRef]
32. Wu, J.; Li, Z.; Luo, X.; Xu, M.; Wu, Y. Intermittency of charged particles in the hybrid UrQMD+CMC model at energies available at the BNL Relativistic Heavy Ion Collider. *Phys. Rev. C* **2022**, *106*, 054905. [CrossRef]
33. Li, Z. Overview of intermittency analysis in heavy-ion collisions. *Mod. Phys. Lett. A* **2022**, *37*, 2230009. [CrossRef]
34. Hwa, R.C.; Nazirov, M.T. Intermittency in second order phase transition. *Phys. Rev. Lett.* **1992**, *69*, 741–744. [CrossRef]
35. Bialas, A.; Peschanski, R.B. Moments of Rapidity Distributions as a Measure of Short Range Fluctuations in High-Energy Collisions. *Nucl. Phys. B* **1986**, *273*, 703–718. [CrossRef]
36. Bialas, A.; Peschanski, R.B. Intermittency in Multiparticle Production at High-Energy. *Nucl. Phys. B* **1988**, *308*, 857–867. [CrossRef]
37. Antoniou, N.G.; Contoyiannis, Y.F.; Diakonos, F.K.; Karanikas, A.I.; Ktorides, C.N. Pion production from a critical QCD phase. *Nucl. Phys. A* **2001**, *693*, 799–824. [CrossRef]
38. Hwa, R.C. Scaling exponent of multiplicity fluctuation in phase transition. *Phys. Rev. D* **1993**, *47*, 2773–2781. [CrossRef]
39. Hwa, R.C.; Yang, C.B. Local Multiplicity Fluctuations as a Signature of Critical Hadronization at LHC. *Phys. Rev. C* **2012**, *85*, 044914. [CrossRef]
40. Ochs, W.; Wosiek, J. Intermittency and Jets. *Phys. Lett. B* **1988**, *214*, 617–620. [CrossRef]
41. Ochs, W. Multidimensional intermittency analysis. *Z. Phys. C* **1991**, *50*, 339–344. [CrossRef]
42. Xie, Y.L.; Chen, G.; Wang, J.L.; Liu, Z.H.; Wang, M.J. Scaling properties of multiplicity fluctuations in heavy ion collisions simulated by AMPT model. *Nucl. Phys. A* **2013**, *920*, 33–44. [CrossRef]
43. Kamal, A.; Ahmad, N.; Khan, M.M. Study of Anomalous Fractal Dimensions and Scaling Exponent in Ginzburg–Landau Phase Transition in 14.5A GeV/c ^{28}Si–AgBr Interactions. *Acta Phys. Polon. B* **2015**, *46*, 1549. [CrossRef]
44. Cao, Z.; Gao, Y.; Hwa, R.C. Scaling properties of hadron production in the Ising model for quark - hadron phase transition. *Z. Phys. C* **1996**, *72*, 661–670. [CrossRef]
45. Prokhorova, D.; Davis, N. Highlights from NA61/SHINE: Proton intermittency analysis. *Universe* **2019**, *5*, 103. [CrossRef]
46. Omana Kuttan, M.; Zhou, K.; Steinheimer, J.; Stoecker, H. Ultrafast, event-by-event heavy-ion simulations for next-generation experiments. *Phys. Rev. C* **2025**, *112*, 054907. [CrossRef]
47. Brofas, A.; Zampetakis, M.; Diakonos, F. Hypercontractivity and factorial moment scaling in the symmetry broken phase. *Phys. Lett. B* **2025**, *863*, 139376. [CrossRef]
48. Wu, J.; Lin, Y.; Wu, Y.; Li, Z. Probing QCD critical fluctuations from intermittency analysis in relativistic heavy-ion collisions. *Phys. Lett. B* **2020**, *801*, 135186. [CrossRef]
49. Wu, Y.F.; Liu, L.S. On the selfaffinity of multiplicity fluctuation in the phase space of multiparticle production. *Phys. Rev. Lett.* **1993**, *70*, 3197–3200. [CrossRef]
50. Agababyan, N.M.; Atayan, M.R.; Charlet, M.; Czyżewski, J.; De Wolf, E.A.; Dziunikowska, K.; Endler, A.M.F.; Garutchava, Z.S.; Gulkanyan, H.R.; Hakobyan, R.S.; et al. Self-affine fractality in pi+ p and K+ p collisions at 250 GeV/c. *Phys. Lett. B* **1996**, *382*, 305–311. [CrossRef]